Mathematical Relationships between Motoneuron Properties Derived by Empirical Data Analysis: Size Determines All Motoneuron Properties

Arnault Caillet[1], Andrew T.M. Phillips[1], Dario Farina[2,*], Luca Modenese[1,*]

[1]Department of Civil and Environmental Engineering, Imperial College London, SW7 2AZ, UK
[2]Department of Bioengineering, Imperial College London, SW7 2AZ, UK

* These authors have equal contributions and share the senior authorship

Corresponding author email: l.modenese@imperial.ac.uk

CONFLICT OF INTEREST STATEMENT: The authors declare no competing financial interests.

ACKNOWLEDGEMENTS: Imperial College Skempton Scholarship to A.C. and Imperial College Research Fellowship to L.M.

Abstract

Our understanding of the behaviour of motoneurons (MNs) in mammals partly relies on our knowledge of the relationships between MN membrane properties, such as MN size, resistance, rheobase, capacitance, time constant, axonal conduction velocity and afterhyperpolarization period. Based on scattered but converging evidence, current experimental studies and review papers qualitatively assumed that some of these MN properties are related. Here, we reprocessed the data from 27 experimental studies in cat and rat MN preparations to empirically demonstrate that all experimentally measured MN properties are associated to MN size. Moreover, we expanded this finding by deriving mathematical relationships between each pair of MN properties. These relationships were validated against independent experimental results not used to derive them. The obtained relationships support the classic description of a MN as a membrane equivalent electrical circuit and describe for the first time the association between MN size and MN membrane capacitance and time constant. The obtained relations indicate that motor units are recruited in order of increasing MN size, muscle unit size, MN rheobase, unit force recruitment thresholds and tetanic forces, but underlines that MN size and recruitment order may not be related to motor unit type.

Keywords: motor neuron, motoneuron, motor neuron size, mathematical relationships, motor unit, Henneman's size principle

Significance statement

This study processed all available experimental data to date to provide the first mathematical and empirical proof that all motoneuron (MN) properties – rheobase, resistance, capacitance, membrane time constant, axonal conduction velocity, afterhyperpolarization period – are directly predictable from MN size. Mathematical relationships between each of these MN properties are derived and validated, and best reproduce the current knowledge in MN properties. For the first time, MN profiles of inter-consistent and motoneuron-specific properties can be built from these equations.

Introduction

Our understanding of the behaviour of motoneurons (MNs) in mammals partly relies on the knowledge of the relationships between MN properties. The most relevant MN properties are reported in Table 1. Direct measurement of some of these properties has been performed in animal studies and yielded some significant correlations. For example, the size of MNs has been found to be strongly associated to the axonal conduction velocity (Cullheim, 1978; Kernell and Zwaagstra, 1981; Burke et al., 1982; Binder et al., 1996).

However, because of technical difficulties in measuring MN properties, measurements have been performed for a limited range of values and for only a few properties concurrently in each study. Our knowledge of MN properties and their associations is therefore limited to a series of datasets that provide a crude picture of MN physiological and biophysical features but not a detailed understanding of the working principles of MNs. For this reason, the statements reported in review papers on the association between MN properties rely on converging conclusions from independent studies and remain speculative (Henneman, 1981; Burke, 1981; Binder et al., 1996; Powers and Binder, 2001; Kernell, 2006; Heckman and Enoka, 2012). While qualitative associations, such as between MN size and resistance (Kernell and Zwaagstra, 1981; Burke et al., 1982), have led to extensions of the Henneman's size principle (Henneman, 1957; Wuerker et al., 1965; Henneman et al., 1965a; Henneman et al., 1965b; Henneman et al., 1974; Henneman, 1981; Henneman, 1985), other relationships, such as between MN size and membrane capacitance or time constant, are not known.

Due to the lack of mathematical descriptions of the relationships between MN properties and size, MN property profiles are typically built with scattered data from a relatively small number of experimental studies. Such generic MN profiles indicate reasonable orders of magnitude but result in a lack of inter-consistency between the MN properties. This approach yields obvious limitations when the sets of physiological and MN-specific characteristics must be known, as in numerical models of a MN membrane equivalent electrical circuit (Negro et al., 2016; Teeter et al., 2018).

To tackle the above limitations in our understanding of MN characteristics, algebraic relationships must be derived between the main MN properties. This can be done either by extrapolating these relationships from existing data or by concurrently measuring all properties in single MNs. The latter approach is currently not possible because of technical constraints which make it impossible to date to experimentally measure a complete and reliable set of MN-specific values for a large sample of MNs. It has been possible in specialised experimental set-ups to measure a maximum of six MN properties concurrently in animal preparations, and for limited ranges of values (Gustafsson and Pinter, 1984a; Gustafsson and Pinter, 1984b). Conversely, these direct measurements are not feasible in humans in vivo, where only axonal conduction velocity can be estimated from indirect measurements (Freund et al., 1975; Dengler et al., 1988).

Here, we derived currently unknown mathematical associations between MN properties by digitizing, reprocessing, and merging the data from 27 available experimental studies in cat and rat preparations. In this way, we first demonstrate that the MN properties reported in Table 1 are all precisely predicted by MN size. Second, we derive mathematical relationships between any pair of the MN properties listed in Table 1. These empirical relationships were validated on new data from studies not used for their derivation and provide for the first time a mathematical framework for the association between any pair of MN properties. Finally, using additional correlations obtained between some MN and muscle unit (mU) properties, we discuss the empirical relationships obtained between MN properties in the context of the Henneman's size principle.

Table 1: The motoneuron (MN) and muscle unit (mU) properties investigated in this study with their notations and SI base units. S_{MN} is the size of the MN. As reproduced in Table 2, the MN size S_{MN} is adequately described by measures of (1) the MN head surface area S_{head}, (2) the soma diameter D_{soma} and (3) the axon diameter D_{axon}. R and R_m define the MN-specific electrical resistance properties of the MN and set the value of the MN-specific current threshold I_{th} (Binder et al., 1996; Powers and Binder, 2001; Heckman and Enoka, 2012). *C and C_m (constant among the MN pool) define the capacitance properties of the MN and contribute to the definition of the MN membrane time constant τ* (Gustafsson, B. and Pinter, 1984b; Zengel et al., 1985). *ΔV_{th} is the constant amplitude of the membrane voltage depolarization threshold relative to resting state required to elicit an action potential. I_{th} is the corresponding electrical current causing a membrane depolarization of ΔV_{th}. AHP is defined in most studies as the duration between the action potential onset and the time at which the MN membrane potential meets the resting state after being hyperpolarized. CV is the axonal conduction velocity of the elicited action potentials on the MN membrane. S_{mU} is the size of the mU. As indicated in Table 2, the mU size S_{mU} is adequately described by measures of (1) the sum of the cross-sectional areas (CSAs) of the fibres composing the mU CSA^{tot}, (2) the mean fibre CSA CSA^{mean}, (3) the innervation ratio IR, i.e. the number of innervated fibres constituting the mU, and (4) the mU tetanic force F^{tet}. The muscle force at which a mU starts producing mU force is called mU force recruitment threshold F^{th}.*

	Properties	**Notation**	**Unit**
Motoneuron (MN) properties	Size:	S_{MN}	
	Head surface area	S_{head}	$[m^2]$
	Soma diameter	D_{soma}	$[m]$
	Axon diameter	D_{axon}	$[m]$
	Resistance	R	$[\Omega]$
	Specific resistance per unit area	R_m	$[\Omega \cdot m^2]$
	Capacitance	C	$[F]$
	Specific capacitance per unit area	C_m	$[F \cdot m^{-2}]$
	Time constant	τ	$[s]$
	Rheobase (current recruitment threshold)	I_{th}	$[A]$
	Voltage threshold	ΔV_{th}	$[V]$
	Afterhyperpolarization period	AHP	$[s]$
	Conduction velocity	CV	$[m \cdot s^{-1}]$
Muscle unit (mU) properties	Size:	S_{mU}	
	Total fibre cross-sectional area (CSA)	CSA^{tot}	$[m^2]$
	Mean fibre CSA	CSA^{mean}	$[m^2]$
	Innervation ratio	IR	[ ]
	Tetanic force	F^{tet}	$[N]$
	Force recruitment threshold	F^{th}	$[N]$

Methods

We analysed the results of the experimental studies in the literature that measured and provided direct comparisons between pairs of the MN properties reported in Table 1. From a first screening of the literature, most of the investigated pairs comprised either a direct measurement of MN size, noted as S_{MN} in this study, or another variable strongly associated to size, such as axonal conduction velocity (CV) or afterhyperpolarization period (AHP). Accordingly, and consistent with the Henneman's size principle, we identify S_{MN} as the reference MN property with respect to which the relationship with the other MN properties in Table 1 is investigated.

For convenience, in the following, the linear relationship between the properties A and B in the form $A = k \cdot B$ with k a constant gain, is noted as $A \propto B$ and reads 'A is linearly related to B'.

Definitions of MN Size S_{MN}, mU size S_{mU} and MU size S_{MU}

In the literature, the MN size S_{MN} is either a conceptual parameter or its definition varies among studies to be the measure of the MN head surface area S_{head} (Burke *et al.*, 1982), the dendritic surface area $S_{dendrites}$ (Barrett and Crill, 1974), the soma diameter D_{soma} (Kernell and Zwaagstra, 1981), or the dendrites cross-sectional area (Kernell, 1966). To avoid confusion and to enable future inter-study comparisons in seeking relationships between S_{MN} and the MN properties reported in Table 1, we here provide a precise definition for S_{MN}. The membrane surface area S_{head} of the head of the MN is an adequate geometrical definition of S_{MN} (Burke, 1981). S_{head} was directly measured in a few animal studies as a spheric soma of diameter D_{soma} and surface S_{soma} connected to cylindric and branching dendrites of individual 1st-order diameters $D_{dendrite}$ and membrane surface $S_{dendrite}$ (Kernell, 1966; Cullheim, 1978; Ulfhake and Kellerth, 1981; Kernell and Zwaagstra, 1981; Burke et al., 1982; Kernell and Zwaagstra, 1989). According to the direct measurements of S_{soma} performed in (Kernell, 1966; Barrett and Crill, 1974; Cullheim, 1978; Zwaagstra and Kernell, 1980; Kernell and Zwaagstra, 1981; Ulfhake and Kellerth, 1981; Burke et al., 1982), the total dendritic surface area $S_{dendrites}$ is found to account for at least 85% of S_{head}, so $S_{head} = S_{soma} + S_{dendrites} \approx S_{dendrites}$. Moreover, as $S_{dendrite} \propto D_{dendrite}$ according to (Ulfhake and Kellerth, 1981), and as the average $D_{dendrite}$ is linearly correlated to D_{soma} (Ulfhake and Kellerth, 1981), we also obtain $S_{dendrites} \propto D_{soma}$. As the axon diameter D_{axon} and D_{soma} are linearly correlated (Cullheim, 1978), overall we obtain that S_{head}, D_{soma} and D_{axon} are linearly related, consistently with previous findings (Burke et al., 1982; Kernell and Zwaagstra, 1989):

$$S_{MN} = S_{head} \propto D_{soma} \propto D_{axon}$$

Consequently, the conceptual MN size S_{MN} is adequately and consistently described by the measurable and linearly inter-related MN head surface area S_{head}, soma diameter D_{soma}, and axon diameter D_{axon}, as reported in Table 2. Therefore, the relationships between MN size S_{MN} and the other MN properties reported Table 1 can be obtained from experimental studies providing measures of S_{head}, D_{soma} and D_{axon}, and not S_{soma} or $D_{dendrite}$ for example.

Similarly, to enable future comparisons between MN and mU properties, we provide a precise definition of the mU size S_{mU}. The size of a mU (S_{mU}) can be geometrically defined as the sum CSA^{tot} of the cross-sectional areas CSAs of the innervated fibres composing the mU. CSA^{tot} depends on the mU innervation ratio (IR) and on the mean CSA (CSA^{mean}) of the innervated fibres: $S_{mU} = CSA^{tot} = IR \cdot CSA^{mean}$. CSA^{tot} was measured in a few studies on cat and rat muscles, either indirectly by histochemical fibre profiling (Burke and Tsairis, 1973; Dum and Kennedy, 1980; Burke, 1981), or directly by glycogen depletion, periodic acid Schiff (PAS) staining and fibre counting (Burke et al., 1982; Bodine et al., 1987; Chamberlain and Lewis, 1989; Totosy de Zepetnek, J E et al., 1992; Kanda and Hashizume, 1992; Rafuse et al., 1997). The mU tetanic force F^{tet} is however more commonly measured in animals. As the fibre mean specific force σ is considered constant among the mUs of one muscle in animals (Bodine et al., 1987; Lucas et al., 1987; Chamberlain and Lewis, 1989; Totosy de Zepetnek, J E et al., 1992; Enoka, 1995), the popular equation $F^{tet} = \sigma \cdot IR \cdot CSA^{mean}$ (Burke, 1981;

Enoka, 1995) returns a linear correlation $F^{tet} \propto IR \cdot CSA^{mean} = S_{mU}$ in animals. Experimental results further provide the relationships $F^{tet} \propto IR$ (Bodine et al., 1987; Chamberlain and Lewis, 1989; Totosy de Zepetnek, J E et al., 1992; Kanda and Hashizume, 1992; Rafuse et al., 1997) and $F^{tet} \propto CSA^{mean}$ (Burke and Tsairis, 1973; Bodine et al., 1987; Totosy de Zepetnek, J E et al., 1992; Kanda and Hashizume, 1992). Consequently, F^{tet}, IR and CSA^{mean} are measurable, consistent, and valid measures of S_{mU} in animals, as summarized in Table 2:

$$S_{mU} = CSA^{tot} \propto CSA^{mean} \propto IR \propto F^{tet}$$

In the following, the MU size S_{MU} can refer to any of the size indices reported Table 2.

Table 2: Reliable and measurable indices of MN, mU and MU sizes in animals. S_{MN}, S_{mU} and S_{MU} are conceptual parameters which are adequately described by the measurable and linearly inter-related quantities reported in this table.

MN size (S_{MN})	mU size (S_{mU})	MU size (S_{MU})
$\boldsymbol{S_{head}}$		S_{head}
$\boldsymbol{D_{soma}}$		D_{soma}
$\boldsymbol{D_{axon}}$		D_{axon}
	F^{tet}	F^{tet}
	IR	IR
	CSA^{mean}	CSA^{mean}
	CSA^{tot}	CSA^{tot}

Relationships between MN properties

For convenience, in the following, the notation $\{A; B\}$ refers to the pair of properties A and B, to which a relationship f can be defined in the form $A = f(B)$.

Digitized data and trendlines

Available studies on MN properties generally provide clouds of data points for pairs $\{A; B\}$ of concurrently measured MN properties through scatter graphs. These plots were digitized using the online tool WebPlotDigitizer (Ankit, 2020). To enable cross-study analysis, the coordinates of the digitized points were then normalized for each study and transformed as a percentage of the maximum property value measured in the same study. The normalized pairs of points for $\{A; B\}$ retrieved from different studies were then merged into a 'global' dataset dedicated to that property pair. A least square linear regression analysis was performed for the $\ln(A) - \ln(B)$ transformation of each global dataset yielding $\ln(A) = a \cdot \ln(B) + k$ relationships which were converted into power relationships of the type $A = k \cdot B^a$, also noted as $A \propto B^a$. Power fitting was chosen for flexibility and simplicity. The adequacy of these global power trendlines and the statistical significance of the correlations were assessed with the coefficient of determination r^2 (squared value of the Pearson's correlation coefficient) and a threshold of 0.05 on the p-value of the regression analysis, respectively. To further assess the reliability of each derived trendline and the inter-study consistency, the equation of the global trendline was compared against the power relationships obtained from individual regression analyses performed for each paper constituting the dataset.

Size-dependent algebraic relationships

Once the $A \propto B^a$ relationships were obtained from trendline fitting for all pairs $\{A; B\}$ found in the literature, the MN properties in Table 1 were processed in a step-by-step manner in the order $CV, AHP, R, I_{th}, C, \tau$ to seek a power relationship $A \propto S_{MN}^c$ between each of them and S_{MN}. For each investigated property A and each fitted $\{A; B\}$ pair, two cases existed. If $B = S_{MN}$, a size-dependent relationship $A \propto S_{MN}^b$ was directly obtained. If $B \neq S_{MN}$, a statistically significant $A \propto B^{a_A}$ relationship was found between properties A and B, and if a power relationship $B \propto S_{MN}^c$ had previously been

derived for the pair $\{B; S_{MN}\}$, a consistent power relationship $A \propto S_{MN}^{a_A \cdot c}$, noted $A \propto S_{MN}^{b}$ was mathematically derived for $\{A; S_{MN}\}$. With this dual approach, as many $A \propto S_{MN}^{b}$ relationships as available $\{A; B\}$ pairs were obtained for the pair $\{A; S_{MN}\}$ for each property A. If the obtained b-values were consistent, i.e. of the same sign and within an arbitrary 3-fold range, it was concluded that property A was correlated to S_{MN} following an $A \propto S_{MN}^{c}$ relationship. In this case, the c-value was calculated as the average of the individual power values b and rounded to the nearest integer. This new $A \propto S_{MN}^{c}$ relationship, called 'final relationship' could be used in the derivation of the next-in-line X property (in the second case), and the steps described above were repeated to seek a new $X \propto S_{MN}^{c}$ final relationship for X.

Scaling the normalized final relationships

The accuracy of the final $A \propto S_{MN}^{c}$ relationships in reproducing existing data from the literature was first assessed against the typical fold range of the property A. Minimum and maximum absolute values for the properties A and S_{MN} were retrieved from the processed studies and from ten additional studies in the literature that, while not providing an analysis of the relations between MN properties (and therefore not being included in the derivation of the equations), reported ranges of experimental values for the analysed MN properties. An experimental ratio q_S^E was calculated, as the average across studies of the ratios of minimum and maximum values measured for S_{MN}. An experimental ratio q_A^E was similarly obtained for the property A. q_A^E was then compared to a third theoretical ratio $q_A^T = (q_S^E)^{|c|}$, with c taken from the final relationship $A \propto S_{MN}^{c}$, as previously derived. If $\frac{q_A^E}{q_A^T}$ was in the range $[0.75\,;1.25]$, the global $A \propto S_{MN}^{c}$ relationship was considered an accurate method to predict the physiological fold range of MN property A from the physiological fold range of S_{MN}.

Then, the intercept k of the normalized final $A = k \cdot S_{MN}^{c}$ relationships was scaled using the average across studies of the minimum and maximum absolute values for A and S_{MN}. Using the additional ten studies is adequate for scaling k and does not affect the quality of the previously fitted trendlines if there is consistency in the property fold ranges between the fitted data and the additional set of experimental data. In this respect, the ratio q_A^F was calculated as q_A^E restricted to the fitted studies, and it was assessed if $\frac{q_A^F}{q_A^E}$ was in the range $[0.75\,;1.25]$. Then, a theoretical range of values for property A $[A_{min};\ A_{max}]$ was built to lie within the average minimum and maximum values of A retrieved from the literature and to fulfil $\frac{A_{max}}{A_{min}} = q_A^T$. A theoretical range for S_{MN} $[(S_{MN})_{min};\ (S_{MN})_{max}]$ was similarly built over the q_S^E-fold range previously derived. Finally, the intercept k in the relationship $A = k \cdot S_{MN}^{c}$ was scaled as:

$$\begin{cases} k = \dfrac{A_{min}}{(S_{MN})_{min}^{c}} \ ; \ c > 0 \\ k = \dfrac{A_{max}}{(S_{MN})_{min}^{c}} \ ; \ c < 0 \end{cases}$$

Relationships between any two MN properties

When a relationship with S_{MN} was obtained for two MN properties A and B, i.e., $A = k_A \cdot S_{MN}^{c_A}$ and $B = k_B \cdot S_{MN}^{c_B}$, a third empirical relationship was mathematically derived for $\{A; B\}$:

$$A = \frac{k_A}{(k_B)^{\frac{c_A}{c_B}}} \cdot (B)^{\frac{c_A}{c_B}} = k \cdot B^{d}$$

This procedure was applied to all possible $\{A; B\}$ pairs in Table 1.

Relationships between MN and mU properties

To assess whether the empirical relationships $A \propto S_{MN}^{c}$ between MN properties A and MN size S_{MN} derived in this study were in accordance with the Henneman's size principle of MU recruitment, we identified a set of twelve experimental studies that concurrently measured a MN property B_{MN} and a muscle unit (mU) property A_{mU} for the same MU. The data obtained for the pairs $\{A_{mU}; B_{MN}\}$ were fitted with power trendlines, as previously described for MN properties, yielding $A_{mU} \propto B_{MN}^{b}$ relationships. Using both the definition of S_{mU} and the $A \propto S_{MN}^{c}$ final relationships derived previously, the $A_{mU} \propto B_{MN}^{b}$ relationships were then mathematically transformed into $S_{mU} \propto S_{MN}^{c}$ relationships. If all c-values were of the same sign, it was concluded that mU and MN sizes were correlated.

Results

We identified 27 experimental studies on cats and rats that report direct comparisons and processable experimental data for the 15 pairs of MN properties and the 5 pairs of one MN and one mU property represented in the bubble diagram of Figure 1(A).

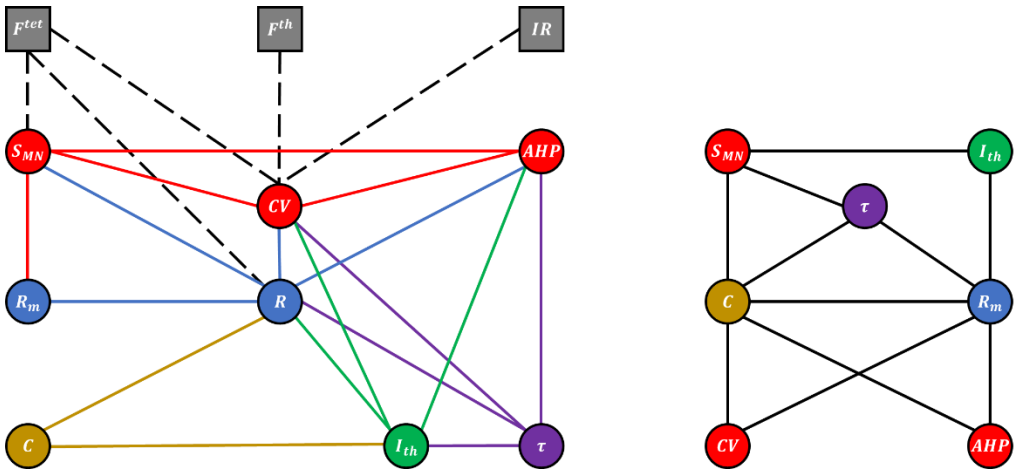

Figure 1: (A) Bubble diagram representing the pairs of MN and/or mU properties that could be investigated in this study from the results provided by 27 experimental studies in the literature. MN and mU properties are represented in circle and square bubbles, respectively. Relationships between MN properties are represented by coloured connecting lines; the colours red, blue, green, yellow and purple are consistent with the order $CV, AHP, R, I_{th}, C, \tau$ in which the pairs were investigated (see Table 3 for mathematical relationships). Relationships between one MN and one mU property are represented by black dashed lines. (B) Bubble diagram representing the mathematical relationships proposed (Table 6) between pairs of MN properties for which no concurrent experimental data has been measured to date.

Relationships between MN properties

The experimental data retrieved for the 15 pairs of MN properties drawn in Figure 1(A) were successfully digitized, normalized, merged into datasets and eventually trendline fitted as reproduced in Figure 2. The equations of the fitted trendlines, the r^2 and p-value of the correlations and the corresponding experimental studies are reported in Table 3. As described in the Methods, this information was step-by-step processed to derive correlations $A \propto S_{MN}^{c}$ (last column of Table 3) between each MN property A reported in Table 1 and MN size S_{MN} in the order $CV, AHP, R, I_{th}, C, \tau$.

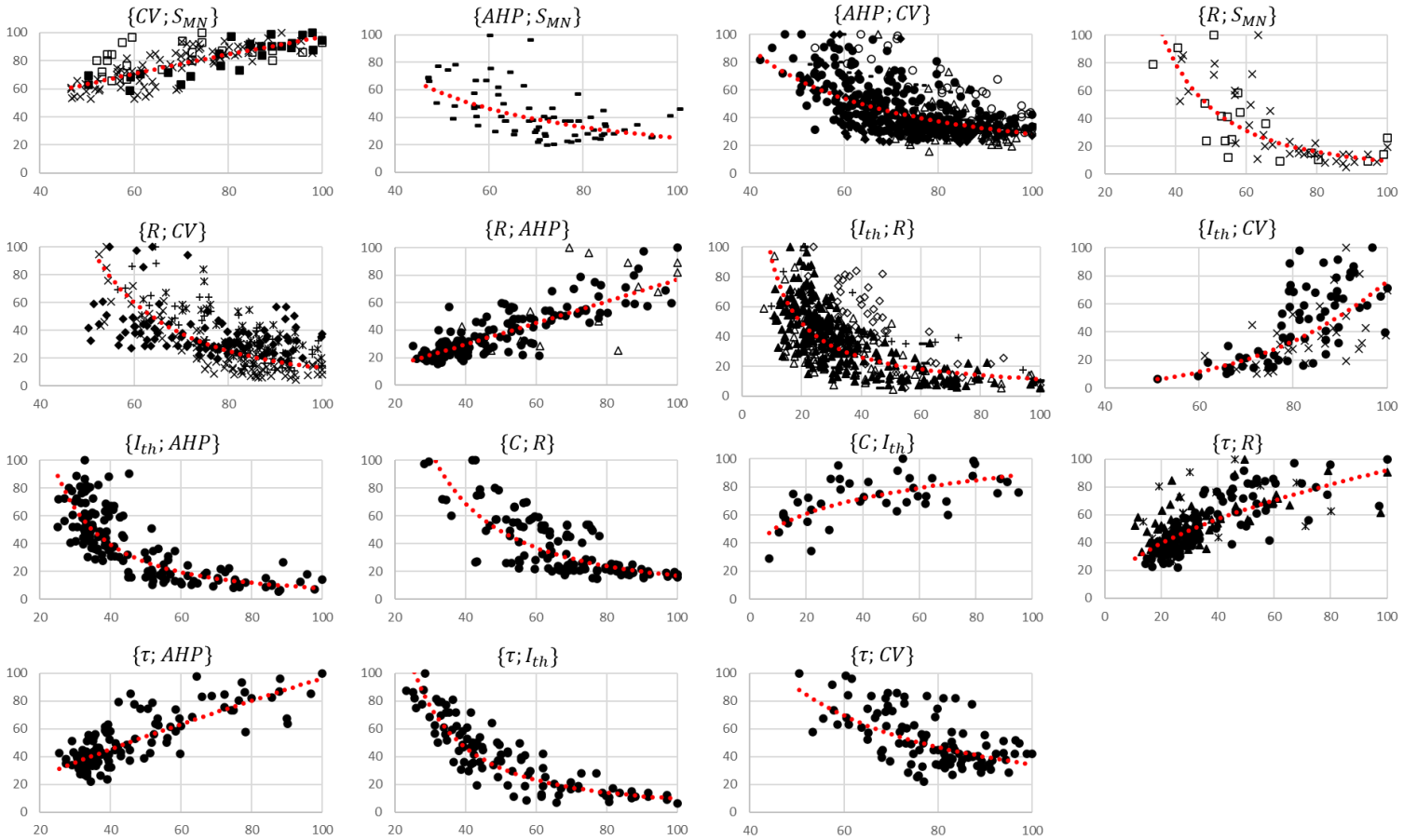

Figure 2: Digitized and normalised data obtained from the 15 experimental studies that measured and investigated the 15 pairs of MN properties reported in Figure 1(A). For each $\{A; B\}$ pair, the property A is read on the y axis and B on the x axis. Trendlines (red dotted curves) are fitted to the data of each dataset as $A = k \cdot B^a$; the equations and r^2 values of the trendlines are reported Table 3. The studies are identified with the following symbols: • (Gustafsson, B. and Pinter, 1984a; Gustafsson, B. and Pinter, 1984b), ○ (Eccles et al., 1957), ▲ (Zengel *et al.*, 1985), Δ (Foehring et al., 1987), ■ (Cullheim, 1978), □ (Burke *et al.*, 1982), ◆ (Gardiner, 1993), ◇ (Fleshman *et al.*, 1981), + (Kernell, 1966)*;* X (Kernell and Zwaagstra, 1981; Kernell and Monster, 1981), - (Zwaagstra and Kernell, 1980), – (Bakels and Kernell, 1993), ✶ (Burke, 1968; Burke and Ten Bruggencate, 1971). *The axes are given in % of the maximum retrieved values in the studies consistently with the Methods section.*

Experimental data for the pair of MN properties $\{CV;\ S_{MN}\}$ was obtained from three studies. As reported in Table 3, the regression trendline returned $r^2 > 0.5$, and the data showed a statistically significant correlation to the level of 0.05. This proved CV to be correlated to S_{MN} following the relationship $CV \propto S_{MN}^{0.6}$ reported in the last column of Table 3. Then, the two pairs of MN properties $\{AHP; S_{MN}\}$ and $\{AHP; CV\}$ were obtained from five studies. The regression trendlines fitted to each pair returned $r^2 = 0.34$ and the data showed a statistically significant correlation to the level of 0.05. From the $\{AHP; S_{MN}\}$ pair, $AHP \propto S_{MN}^{-1.2}$ was directly obtained from the trendline fitting. The fitted $\{AHP; CV\}$ pair returned $AHP \propto CV^{-1.3}$; from the prior information that $CV \propto S_{MN}^{0.6}$, it mathematically yielded $AHP \propto S_{MN}^{-0.8}$. Consequently, two $AHP \propto S_{MN}^{c}$ relationships were obtained for the $\{AHP; S_{MN}\}$ pair with $c \in \{-0.8;\ -1.2\}$, as reported in Table 3. All c-values being negative and within a 1.5-range fold, a global relationship $AHP \propto S_{MN}^{-1}$ was derived (last column of Table 3), following the procedure described in the Methods section. The same procedure was then step-by-step applied to properties R, I_{th}, C and τ. In this respect, three pairs $\{R; CV\}$, $\{R; AHP\}$, $\{R; S_{MN}\}$, three pairs $\{I_{th}; CV\}$, $\{I_{th}; AHP\}$, $\{I_{th}; R\}$, two pairs $\{C; R\}$, $\{C; I_{th}\}$, and four pairs $\{\tau; CV\}$, $\{\tau; AHP\}$, $\{\tau; I_{th}\}$, $\{\tau; R\}$ were processed from seven, seven, two and four studies respectively, yielding twelve statistically significant correlations and regression trendlines with $r^2 \in [0.36; 0.72]$, as shown in Table 3. Size-dependent relationships were again successfully derived between the properties R, I_{th}, C and τ and S_{MN} and listed in the last column of Table 3. These results demonstrate that the MN properties CV, AHP, R, I_{th}, C and τ are correlated to the MN size S_{MN}, and that the size-dependent normalized variations of these MN properties can be described by the power relationships reported in the last column of Table 3 (last column) and plotted in Figure 3. While the relationships obtained for some pairs of MN properties, such as $\{AHP;\ S_{MN}\}$, $\{C; I_{th}\}$ or $\{\tau; CV\}$, relied on a single experimental study, the step-by-step methodology applied here still ensured that the size-dependent relationships (last column of Table 3) relied on two to eight individual studies, enhancing the robustness of these relationships to best describe the available data.

Table 3: Fitted experimental data of pairs of MN properties and subsequent size-dependent relationships. The r^2, p-value and the equation $A \propto B^a$ of the trendlines are reported for each pair of MN properties. An equivalent MN-size related relationships $A \propto S_{MN}^b$ is mathematically derived from each $A \propto B^a$ relationship using, when relevant, knowledge of the previously derived final relationships $X \propto S_{MN}^c$ reported in the last column of this table. The ratio of maximum (100) and minimum normalized values of the fitted datasets shown Figure 2 are also reported for each property.

MN property	$A \propto B^a$ (fitted relationships)						$A \propto S_{MN}^b$ (MN-size related relationships)	$A \propto S_{MN}^c$ (final relationships)
A	Relationship	Ranges A-fold B-fold	a	r^2	p-value	Reference studies	b	
CV	$CV \propto S_{MN}^a$	2.1 1.9	0.6	0.55	$p < 10^{-5}$	(Cullheim, 1978; Kernell and Zwaagstra, 1981; Burke et al., 1982)	0.6	$CV \propto S_{MN}^{0.6}$
AHP	$AHP \propto S_{MN}^a$	5.0 2.2	−1.2	0.34	$p < 10^{-5}$	(Zwaagstra and Kernell, 1980)	−1.2	$AHP \propto S_{MN}^{-1}$
	$AHP \propto CV^a$	6.3 2.4	−1.3	0.34	$p < 10^{-5}$	(Eccles et al., 1957; Zwaagstra and Kernell, 1980; Gustafsson, B. and Pinter, 1984a; Foehring et al., 1987; Gardiner, 1993)	−0.8	
R	$R \propto S_{MN}^a$	19.1 3.0	−2.3	0.60	$p < 10^{-5}$	(Kernell and Zwaagstra, 1981; Burke et al., 1982)	−2.3	$R \propto S_{MN}^{-2}$
	$R \propto CV^a$	22.7 2.0	−3.0	0.36	$p < 10^{-5}$	(Kernell, 1966; Burke, 1968; Kernell and Zwaagstra, 1981; Gardiner, 1993)	−1.8	
	$R \propto AHP^a$	6.4 4.0	1.0	0.66	$p < 10^{-5}$	(Gustafsson, B. and Pinter, 1984a; Foehring et al., 1987)	−1.0	
I_{th}	$I_{th} \propto R^a$	23.3 13.5	−0.9	0.45	$p < 10^{-5}$	(Kernell, 1966; Fleshman et al., 1981; Zengel et al., 1985; Foehring et al., 1987; Bakels and Kernell, 1993)	1.8	$I_{th} \propto S_{MN}^2$
	$I_{th} \propto CV^a$	14.7 2.0	3.7	0.50	$p < 10^{-5}$	(Kernell and Monster, 1981; Gustafsson, B. and Pinter, 1984b)	2.2	
	$I_{th} \propto AHP^a$	17.5 4.0	−1.7	0.72	$p < 10^{-5}$	(Gustafsson, B. and Pinter, 1984b)	1.7	
C	$C \propto R^a$	6.9 3.5	−0.7	0.57	$p < 10^{-5}$	(Gustafsson, B. and Pinter, 1984a)	1.4	$C \propto S_{MN}$
	$C \propto I_{th}^a$	3.4 14.7	0.6	0.42	$p < 10^{-5}$	(Gustafsson, B. and Pinter, 1984b)	1.2	
τ	$\tau \propto R^a$	4.5 9.3	0.5	0.48	$p < 10^{-5}$	(Burke and Ten Bruggencate, 1971; Gustafsson, B. and Pinter, 1984a; Zengel et al., 1985)	−1.0	$\tau \propto S_{MN}^{-1}$
	$\tau \propto AHP^a$	4.7 3.9	0.8	0.59	$p < 10^{-5}$	(Gustafsson, B. and Pinter, 1984a)	−0.8	
	$\tau \propto I_{th}^a$	4.3 15.4	−0.6	0.76	$p < 10^{-5}$	(Gustafsson, B. and Pinter, 1984b)	−1.2	
	$\tau \propto CV^a$	4.7 2.0	−1.4	0.32	$p < 10^{-5}$	(Gustafsson, B. and Pinter, 1984a)	−0.8	

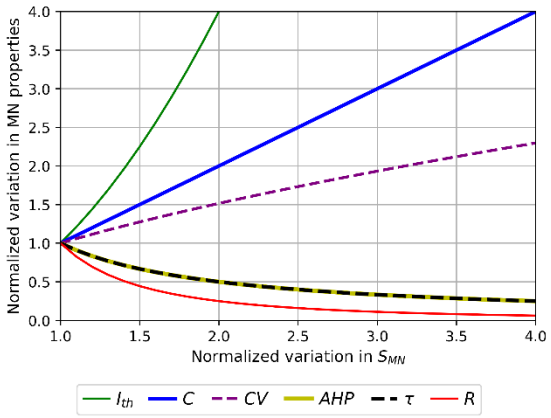

Figure 3: Normalized size-dependent behaviour of the MN properties CV, AHP, R, I_{th}, C and τ. For displaying purposes, the MN properties are plotted in arbitrary units as power functions (intercept $k = 1$) of S_{MN}: $A = S_{MN}^{c}$ according to Table 3. The larger the MN size, the larger CV, C and I_{th} in the order of increasing slopes, and the lower AHP, τ and R in the order of increasing slopes.

For each property A, the size-dependent relationship $A \propto S_{MN}^{c}$ was validated against the typical fold ranges of experimental values for A and S_{MN}, provided in Table 4 and Table 5. D_{soma} and S_{head} were found to vary over an average $q_S^E = 4$-fold range according to a review of the studies reported in Table 4. However, as D_{axon} was previously found to be linearly related to D_{soma} and S_{head}, the value $q_S^E = 2.2$ reported in Table 4 for D_{axon} is inconsistent with $q_S^E = 4$. As the measurements of D_{axon} were performed in only two studies and on datasets of relatively small sizes, the results for D_{axon} were disregarded and S_{MN} was set to vary over a 4-fold range in the following, consistently with Binder et al. (1996).

Table 4: Typical ranges of physiological values for the measures of MN size D_{soma}, D_{axon} and S_{head} according to the reference studies that include the fitted studies and 4 additional studies that did not provide direct comparisons between MN properties. S_{MN} is found to vary over an average $q_S^E = 4$-fold range, which sets the amplitude of the theoretical ranges. Absolute {min; max} reports the minimum and maximum values retrieved in the reference studies for D_{soma}, D_{axon} and S_{head}, while average {min; max} is obtained as the average across reference studies of minimum and maximum values retrieved per study.

Property	Unit	Absolute {min;max}	Average {min; max}	q_S^E	Reference studies	Theoretical range
D_{soma}	$[\mu m]$	$\{15; 230\}$	$\{33.4; 95.9\}$	4	(Kernell, 1966; Cullheim, 1978; Zwaagstra and Kernell, 1980; Kernell and Zwaagstra, 1981; Ulfhake and Kellerth, 1981; Burke et al., 1982)	$[26; 104]$
D_{axon}	$[\mu m]$	$\{4; 10.3\}$	$\{4.2; 9.4\}$	2.2	(Cullheim, 1978; Ulfhake and Kellerth, 1984)	N/A
S_{head}	$[mm^2]$	$\{0.08; 0.75\}$	$\{0.14; 0.53\}$	4.1	(Barrett and Crill, 1974; Ulfhake and Kellerth, 1981; Burke et al., 1982; Ulfhake and Kellerth, 1984)	$[0.13; 0.52]$

Then, the empirical q_A^E and theoretical q_A^T ratios, defined in the Methods, were calculated for each MN property A and are reported in Table 5. For example, MN resistance R was found to vary over an average $q_R^E = 13.8$-fold range in a MN pool according to the literature, while the theoretical fold range $q_R^T = (q_S^E)^{|c_R|} = 4^2 = 16$ was obtained from the $R \propto S_{MN}^{-2}$ relationship previously derived when a 4-fold range is set for S_{MN}. As shown in Table 5, $\frac{q_A^E}{q_A^T} \in [0.75; 1.25]$ for all MN properties $R, R_m, C, \tau, I_{th}, AHP$ and CV. It was therefore concluded that the normalized relationships $A \propto S_{MN}^{c}$ provided in the last column of Table 3 adequately predict the physiological fold range of all MN properties. When q_A^E was directly calculated (results not shown here) from the ten additional experimental studies that were not included in the derivation of the $A \propto S_{MN}^{c}$ relationships, it was still observed $\frac{q_A^E}{q_A^T} \in [0.75; 1.25]$. This

provides a validation of the physiological fold ranges for all MN properties A predicted by the $A \propto S_{MN}^{c}$ relationships.

Table 5: Typical ranges of physiological values for the MN properties R, R_m, C, τ, I_{th}, AHP and CV according to the reference studies. As described in the Methods section, q_A^E is the average among reference studies of the ratios of minimum and maximum values; the properties experimentally vary over a q_A^E-fold range. This ratio compares with the theoretical ratio $q_A^T = (q_S^E)^{|c|}$ (with c taken from Table 3), which sets the amplitude of the theoretical ranges. Absolute and average {min; max} are obtained as described in Table 4. The average fold ranges q_A^F obtained from the fitted data plotted in Figure 2 is compared to q_A^E for future scaling of the intercept k.

MN property	Unit	Fitted fold-range $q_A^F \pm s.d.$	Absolute exp {min;max}	Average exp {min; max}	q_A^E	$\frac{q_A^F}{q_A^E}$	Reference studies	q_A^T	$\frac{q_A^E}{q_A^T}$	Theoretical range
R	$M\Omega$	14.2 ± 4.0	{0.1; 8}	{0.37; 4.4}	13.8	1.03	(Kernell, 1966; Burke, 1968; Burke and Ten Bruggencate, 1971; Kernell and Zwaagstra, 1981; Fleshman et al., 1981; Glenn and Dement, 1981; Burke et al., 1982; Ulfhake and Kellerth, 1984; Gustafsson, B. and Pinter, 1984a; Zengel et al., 1985; Foehring et al., 1986; Foehring et al., 1987; Bakels and Kernell, 1993; Gardiner, 1993)	16	0.86	[0.3; 4.8]
R_m	$\Omega \cdot m^2$	N/A	{0.1; 1.6}	{0.21; 0.79}	3.2	N/A	(Albuquerque and Thesleff, 1968; Barrett and Crill, 1974; Burke et al., 1982; Gustafsson, B. and Pinter, 1984a; Kernell and Zwaagstra, 1989)	4	0.8	[0.16; 0.62]
C	nF	4.9 ± 1.8	{2.2; 8.5}	{2.4; 8.5}	3.9	1.25	(Gustafsson, B. and Pinter, 1984a; Gustafsson, B. and Pinter, 1985)	4	0.98	[2.3; 9.4]
τ	ms	4.6 ± 0.2	{2; 14.2}	{2.7; 10.3}	4	1.15	(Burke and Ten Bruggencate, 1971; Barrett and Crill, 1974; Ulfhake and Kellerth, 1984; Gustafsson, B. and Pinter, 1984a; Zengel et al., 1985; Gustafsson, B. and Pinter, 1985)	4	1.00	[2.9; 11.5]
I_{th}	nA	17.1 ± 3.3	{0.9; 53}	{2; 31}	16.8	1.02	(Kernell, 1966; Fleshman et al., 1981; Kernell and Monster, 1981; Ulfhake and Kellerth, 1984; Gustafsson, B. and Pinter, 1984b; Zengel et al., 1985; Foehring et al., 1986; Foehring et al., 1987; Bakels and Kernell, 1993; Gardiner, 1993)	16	1.05	[2.0; 32.4]
AHP	ms	4.6 ± 0.9	{14; 270}	{39; 171}	4.8	0.96	(Eccles et al., 1957; Gustafsson, Bengt, 1979; Dum and Kennedy, 1980; Zwaagstra and Kernell, 1980; Ulfhake and Kellerth, 1984; Gustafsson, B. and Pinter, 1984a; Zengel et al., 1985; Gustafsson, B. and Pinter, 1985; Foehring et al.,	4	1.2	[42; 168]

							1987; Bakels and Kernell, 1993)				
CV	$m \cdot s^{-1}$	2.1 ± 0.2	$\{10; 150\}$	$\{56; 114\}$	2.7	0.78	(Eccles et al., 1957; McPhedran et al., 1965; Olson and Swett Jr, 1966; Kernell, 1966; Appelberg and Emonet-Dénand, 1967; Burke, 1968; Barrett and Crill, 1974; Proske and Waite, 1974; Bagust, 1974; Stephens and Stuart, 1975; Cullheim, 1978; Dum and Kennedy, 1980; Zwaagstra and Kernell, 1980; Kernell and Zwaagstra, 1981; Fleshman et al., 1981; Glenn and Dement, 1981; Burke et al., 1982; Gustafsson, B. and Pinter, 1984a; Zengel et al., 1985; Foehring et al., 1986; Foehring et al., 1987; Gardiner, 1993)	2.3	1.17	$[51; 117]$

Then, the normalized $A \propto S_{MN}^{c}$ relationships were scaled using typical values for A and S_{MN} obtained from the fitted studies and the ten additional experimental studies. It can be observed in Table 5 that both the processed studies and the extended set of studies return similar fold ranges q_A^F and q_A^E respectively for each property A ($\frac{q_A^F}{q_A^E} \in [0.75; 1.25]$). It is therefore concluded that the additional information provided by the extended set of studies could be adequately used to scale the k-value of the intercept in the normalized $A = k \cdot S_{MN}^{c}$ relationships. To perform the scaling, theoretical ranges of values for $R, R_m, C, \tau, I^{th}, AHP$ and CV were first derived in Table 5 (last column) as described in the Methods. Then, taking the $\{R; S_{head}\}$ pair as example, as $R \propto S_{head}^{-2}$, $R \in [0.3; 4.8] \cdot 10^6 \Omega$ and $S_{head} \in [0.13; 0.52] \cdot 10^{-6} m^2$, it directly yielded from the Methods that $R = \frac{8.1 \cdot 10^{-8}}{S_{head}^2}$ in SI base units. A similar approach yielded the mathematical relationships reported in the two first lines and columns of Table 6 between the MN properties $CV, AHP, R, I_{th}, C, \tau$ and MN size S_{MN}.

Lastly, these size-dependent relationships were used to mathematically derive algebraic relationships between any of the MN properties $R, C, \tau, I^{th}, R_m, AHP$ and CV populating Table 6. Taking the $\{I_{th}; R\}$ pair as example, as $R = \frac{8.1 \cdot 10^{-8}}{S_{head}^2}$ and $S_{head} = 2.9 \cdot 10^{-3} \cdot I_{th}^{0.5}$, the relationship $R = \frac{10^{-2}}{I^{th}} = \frac{\Delta V^{th}}{I^{th}}$ was obtained. All constants and relationships are given in SI base units. The specific capacitance C_m and the membrane voltage threshold ΔV_{th} were found to be constant among MNs, a property discussed in the Discussion section.

Table 6: Mathematical empirical relationships between the MN properties $S_{head}, D_{soma}, R, R_m, C, \tau, I^{th}$, AHP and CV. Each column provides the relationships between one and the eight other MN properties. If one property is known, the complete MN profile can be reconstructed by using the pertinent line in this table. All constants and properties are provided in SI base units (meters, seconds, ohms, farads and ampers).

	$S_{head}[m^2]$	$D_{soma}[m]$	$R[\Omega]$	$R_m[\Omega \cdot m^2]$	$C[F]$	$\tau[s]$	$I_{th}[A]$	$AHP[s]$	$CV[m \cdot s^{-1}]$
$S_{head}[m^2]$		$D_{soma} = 200 \cdot S_{head}$	$R = \frac{8.1 \cdot 10^{-8}}{S_{head}^2}$	$R_m = \frac{8.1 \cdot 10^{-8}}{S_{head}}$	$C = 1.8 \cdot 10^{-2} \cdot S_{head}$	$\tau = \frac{1.5 \cdot 10^{-9}}{S_{head}}$	$I^{th} = 1.2 \cdot 10^5 \cdot S_{head}^2$	$AHP = \frac{2.2 \cdot 10^{-8}}{S_{head}}$	$CV = 6.9 \cdot 10^5 \cdot S_{head}^{0.6}$
$D_{soma}[m]$	$S_{head} = 5 \cdot 10^{-3} \cdot D_{soma}$		$R = \frac{3.2 \cdot 10^{-3}}{D_{soma}^2}$	$R_m = \frac{1.6 \cdot 10^{-5}}{D_{soma}}$	$C = 9.0 \cdot 10^{-5} \cdot D_{soma}$	$\tau = \frac{3.0 \cdot 10^{-7}}{D_{soma}}$	$I^{th} = 3.0 \cdot D_{soma}^2$	$AHP = \frac{4.4 \cdot 10^{-6}}{D_{soma}}$	$CV = 2.9 \cdot 10^4 \cdot D_{soma}^{0.6}$
$R[\Omega]$	$S_{head} = \frac{2.9 \cdot 10^{-4}}{R^{0.5}}$	$D_{soma} = \frac{5.7 \cdot 10^{-2}}{R^{0.5}}$		$R_m = 2.9 \cdot 10^{-4} \cdot R^{0.5}$	$C = \frac{5.1 \cdot 10^{-6}}{R^{0.5}}$	$\tau = 5.3 \cdot 10^{-6} \cdot R^{0.5}$	$I^{th} = \frac{10^{-2}}{R}$	$AHP = 7.7 \cdot 10^{-5} \cdot R^{0.5}$	$CV = \frac{5.1 \cdot 10^3}{R^{0.3}}$
$R_m[\Omega \cdot m^2]$	$S_{head} = \frac{8.1 \cdot 10^{-8}}{R_m}$	$D_{soma} = \frac{1.6 \cdot 10^{-5}}{R_m}$	$R = 1.2 \cdot 10^7 \cdot R_m^2$		$C = \frac{1.4 \cdot 10^{-9}}{R_m}$	$\tau = 1.8 \cdot 10^{-2} \cdot R_m$	$I^{th} = \frac{8.1 \cdot 10^{-10}}{R_m^2}$	$AHP = 2.7 \cdot 10^{-1} \cdot R_m$	$CV = \frac{39}{R_m^{0.6}}$
$C[F]$	$S_{head} = 55.6 \cdot C$	$D_{soma} = 1.2 \cdot 10^4 \cdot C$	$R = \frac{2.4 \cdot 10^{-11}}{C^2}$	$R_m = \frac{1.4 \cdot 10^{-9}}{C}$		$\tau = \frac{2.6 \cdot 10^{-11}}{C}$	$I^{th} = 4.1 \cdot 10^8 \cdot C^2$	$AHP = \frac{3.7 \cdot 10^{-10}}{C}$	$CV = 8.0 \cdot 10^6 \cdot C^{0.6}$
$\tau[s]$	$S_{head} = \frac{1.5 \cdot 10^{-9}}{\tau}$	$D_{soma} = \frac{3.0 \cdot 10^{-7}}{\tau}$	$R = 3.5 \cdot 10^{10} \cdot \tau^2$	$R_m = 55.6 \cdot \tau$	$C = \frac{2.7 \cdot 10^{-11}}{\tau}$		$I^{th} = \frac{2.7 \cdot 10^{-13}}{\tau^2}$	$AHP = 14 \cdot \tau$	$CV = \frac{3.5}{\tau^{0.6}}$
$I_{th}[A]$	$S_{head} = 2.9 \cdot 10^{-3} \cdot I_{th}^{0.5}$	$D_{soma} = 0.57 \cdot I_{th}^{0.5}$	$R = \frac{10^{-2}}{I^{th}}$	$R_m = \frac{2.8 \cdot 10^{-5}}{I_{th}^{0.5}}$	$C = 5.2 \cdot 10^{-5} \cdot I_{th}^{0.5}$	$\tau = \frac{5.2 \cdot 10^{-7}}{I_{th}^{0.5}}$		$AHP = \frac{7.4 \cdot 10^{-6}}{I_{th}^{0.5}}$	$CV = 2.1 \cdot 10^4 \cdot I_{th}^{0.3}$
$AHP[s]$	$S_{head} = \frac{2.2 \cdot 10^{-8}}{AHP}$	$D_{soma} = \frac{4.3 \cdot 10^{-6}}{AHP}$	$R = 1.7 \cdot 10^8 \cdot AHP^2$	$R_m = 3.7 \cdot AHP$	$C = \frac{3.8 * 10^{-10}}{AHP}$	$\tau = 6.9 \cdot 10^{-2} \cdot AHP$	$I^{th} = \frac{5.6 * 10^{-11}}{AHP^2}$		$CV = \frac{17}{AHP^{0.6}}$
$CV[m \cdot s^{-1}]$	$S_{head} = 1.6 \cdot 10^{-10} \cdot CV^{1.7}$	$D_{soma} = 3.3 \cdot 10^{-8} \cdot CV^{1.7}$	$R = \frac{2.1 \cdot 10^{12}}{CV^{3.3}}$	$R_m = \frac{5.0 \cdot 10^2}{CV^{1.7}}$	$C = 2.9 \cdot 10^{-12} \cdot CV^{1.7}$	$\tau = \frac{9.2}{CV^{1.7}}$	$I^{th} = 4.7 \cdot 10^{-15} \cdot CV^{3.3}$	$AHP = \frac{1.4 \cdot 10^2}{CV^{1.7}}$	

The mathematical relationships in Table 6 are reliable in explaining all the existing data retrieved from the literature. First, they remain consistent (Table 7) with the power relationships that were experimentally derived in the studies listed in Table 3 for the pairs $\{I_{th}; R\}, \{C; R\}, \{C;\ I_{th}\}, \{\tau; R\}$ and $\{\tau; I_{th}\}$. In Table 7, experimental and empirical c-values show a strong match for the 5 pairs of MN properties, demonstrating that the empirical relationships derived in this study are expedient in predicting the inter-relationships between MN properties.

Table 7: Table reporting the power relationships obtained for the 5 pairs $\{I_{th}; R\}, \{C; R\}, \{I_{th}; C\}, \{I_{th}; \tau\}$ and $\{\tau; R\}$ of MN properties that were concurrently investigated in the literature and that did not included direct measures or indices (CV, AHP) of MN size. The c-values obtained from the fitted data and reported Table 3 (in which there are named a) and the c-values obtained from the empirical relationships derived Table 6 are consistent for the 5 pairs.

Relationship	c-value (fitted relationships)	c-value (mathematical relationships)
$I^{th} \propto R^c$	-0.9	-1
$C \propto R^c$	-0.7	-0.5
$C \propto I_{th}^c$	0.6	0.5
$\tau \propto R^c$	0.5	0.5
$\tau \propto I_{th}^c$	-0.6	-0.5

The mathematical relationships in Table 6 are moreover strongly consistent with further experimental measurements that were not included in the data processing used for deriving our relationships and displayed in Figure 2. The relationships $I^{th} \propto \frac{1}{\tau^2}$, $\frac{1}{C} \propto \tau$, $S_{MN} \propto CV$ and $R \propto \frac{1}{S_{MN}^2}$ (Table 6) are, when combined, perfectly consistent with the relationship $\frac{I^{th}}{C} \propto \frac{1}{\tau}$ experimentally observed in Gustafsson and Pinter (1985) and $\frac{1}{R \cdot S_{MN}} \propto CV$ measured in Kernell and Zwaagstra (1981). No correlation between $\frac{\Delta V_{th}}{R \cdot I_{th}}$ and C is reported by the empirical relationships in Table 6, consistent with measurements performed in Gustafsson, B. and Pinter (1984b), substantiating that the dynamics of MN recruitment dominantly rely on R, I^{th} and ΔV_{th} (Heckman and Enoka, 2012). The stronger-than-linear inverse relationship $R \propto \frac{1}{S_{MN}^2}$ is consistent with the phenomenological conclusions from Kernell and Zwaagstra (1981). Similarly, the retrieved $R_m \propto \frac{1}{S_{MN}}$ relationship is consistent with the modelling conclusions from Barrett and Crill (1974), who reported a significant $R_m \propto R \cdot S_{MN}$ relationship and a weak but significant $R_m \propto \frac{1}{S_{MN}}$ relationship. The indirect conclusion on a positive correlation between R_m and AHP in Gustafsson and Pinter (1984b) is finally consistent with $R_m \propto AHP$ (Table 6). However, interestingly, the relationship $R_m \propto \frac{1}{S_{MN}}$ contradicts the speculations in Kernell and Zwaagstra (1981) and Gustafsson and Pinter (1984b) that R_m is the dominant factor influencing the distribution of R values rather than S_{MN}.

This study also predicts the correlations between MN properties that were either never reported in past review studies, such as the positive $S_{MN} - \tau$ relationship, or never concurrently measured in the literature, as displayed in Figure 1(B). Such unknown relationships were indirectly extracted from the combination of known relationships (Table 3) and typical ranges of values obtained from the literature for these properties. For example, $I_{th} \propto S_{MN}^2$ was predicted from the following combinations of known and validated relationships: $\{I_{th} \propto R^{-1}; R \propto S_{MN}^{-2}\}$, or $\{I^{th} \propto AHP^{-2}; AHP \propto S_{MN}\}$. Due to the prior validation of the relationships in Table 6, these findings are reliable as indirectly consistent with the literature data processed in this study and provide new insights on the size-dependency of the MN recruitment mechanisms.

Relationships between MN and mU properties

As shown in Figure 1(A), five pairs of one MN and one mU property were investigated in twelve studies in the literature in cats and rats, and none in the past 30 years, as remarked by Heckman and Enoka

(2012). One study on the rat gastrocnemius muscle (Kanda and Hashizume, 1992) indicated no correlation between IR and CV. However, after removing from the dataset 2 outliers that fell outside two standard deviations of the mean data, a statistically significant correlation ($p < 0.05$) between IR and CV was successfully fitted with a power trendline ($r^2 = 0.43$). Eight studies, dominantly focusing on the cat soleus and medial gastrocnemius muscles, found a strong correlation between F^{tet} and CV, while one study showed a significant correlation for the pair $\{F^{tet}; R\}$ in both the cat tibialis anterior and extensor digitorum longus muscles. Finally, one study (Burke *et al.*, 1982) on the cat soleus, medial and lateral gastrocnemius muscles inferred a statistically significant correlation for $\{F^{tet}; S_{MN}\}$. As F^{tet} and IR are reliable indices of S_{mU}, by using the MN relationships in Table 3, four $S_{mU} \propto S_{MN}^{c}$ relationships were obtained between mU and MN properties (Table 8), and returned a 2.2-fold range in positive c-values $c \in [2.0; 4.3]$.

Table 8: Fitted experimental data of pairs of one mU and one MN property and subsequent $S_{mU} \propto S_{MN}^{c}$ relationships. The r^2, p-value and the equation $A \propto B^c$ of the trendlines are reported for each pair of properties. In the last column, prior knowledge is used to derive $S_{mU} \propto S_{MN}^{c}$ relationships.

Species	$A \propto B^c$ (fitted relationships)					$S_{mU} \propto S_{MN}^{c}$ (final relationships)
	Relationship	c	r^2	p-value	Reference studies	c
Rat	$IR \propto CV^c$	3.4	0.45	0.006	(Kanda and Hashizume, 1992)	2.0
Cat	$F^{tet} \propto CV^c$	7.2	0.37	$p < 10^{-5}$	(McPhedran et al., 1965; Wuerker et al., 1965; Appelberg and Emonet-Dénand, 1967; Proske and Waite, 1974; Bagust, 1974; Jami and Petit, 1975; Stephens and Stuart, 1975; Burke et al., 1982; Emonet-Dénand et al., 1988)	4.3
	$F^{tet} \propto R^c$	−1.3	0.27	$6 \cdot 10^{-5}$	(Dum and Kennedy, 1980)	2.6
	$F^{tet} S_{MN}^{c}$	2.0	0.21	0.02	(Burke *et al.*, 1982)	2.0

Discussion

We processed the data from previous experimental studies to extract mathematical relationships between several MN properties and MN size. This allowed us to demonstrate that all investigated MN properties are predicted by MN size and that properties at the level of individual MNs are interrelated. We established mathematical relations linking all the pairs of MN properties (Table 6). These relationships were validated with respect to the ranges of the predicted MN properties against a set of typical literature range values (Table 5), against directly fitted experimental data (Table 7) and against other results available in the literature.

The findings are consistent with considerations from previous papers and literature reviews, either drawn from direct but isolated measurements or speculated. For example, Binder et al. (1996) concluded that the AHP duration was inversely related to MN size S_{MN} based on measures of a single experimental study. Conversely, the size-dependencies of R and I_{th} were qualitatively assumed by Powers and Binder (2001) from the equations obtained from a variant of the Rall's model of MN membrane equivalent electrical circuit, and not from experimental data. The negative correlation between S_{MN} and R was predicted by Binder et al. (1996) from the findings of Henneman's studies on the correlation between extracellular spike amplitude and S_{MN} (Henneman, 1957; Henneman et al., 1965a). The fact that R defines the MN rheobase and thus dictates the size order of MN recruitment was similarly justified in Binder et al. (1996) and Powers and Binder (2001) from a combination of Henneman's findings and Rall's model equations. Moreover, all previous papers used the debated association between MU type and S_{MN}, mainly obtained from measures in the cat gastrocnemius muscle (Fleshman et al., 1981; Burke et al., 1982; Zengel et al., 1985; Bakels and Kernell, 1993), to indirectly speculate on correlations between S_{MN} and AHP (Heckman and Enoka, 2012), R (Powers and Binder, 2001; Heckman and Enoka, 2012), R_m (Binder et al., 1996; Powers and Binder, 2001) or I_{th} (Binder et al., 1996). Finally, we could find a single paper that inferred a positive correlation between S_{MN} and C (Heckman and Enoka, 2012) but without reference to direct experimental results.

Relevance for MN modelling

The empirical equations in Table 6 support the common approach of modelling the MN membrane behaviour with an equivalent resistance-capacitance electrical circuit as variants of the Rall's cable model (Rall, 1957; Rall, 1959; Rall, 1960). The relationship between C and S_{MN} reported in Table 6 validates the definition $C = C_m \cdot S_{MN}$, as well as it emphasizes that the specific capacitance C_m per unit area is constant among the MN pool, and indirectly yields, from typical ranges of C and S_{MN} in the literature, the relation $C_m = 1.8 \cdot 10^{-2} F \cdot m^{-2}$, which is highly consistent with the average ranges of values reported in (Lux and Pollen, 1966; Albuquerque and Thesleff, 1968; Barrett and Crill, 1974; Adrian and Hodgkin, 1975; Sukhorukov et al., 1993; Major et al., 1994; Solsona et al., 1998; Thurbon et al., 1998; Gentet et al., 2000). Similarly, the empirical relationship $I_{th} = \frac{10^{-2}}{R}$ (Table 6) yields $\Delta V_{th} = 10mV$, consistently with (Brock et al., 1952; Eccles et al., 1958), despite uncertainties in the value of the membrane resting potential (Heckman and Enoka, 2012). This supports the conclusions that the relative voltage threshold ΔV_{th} is constant within the MN pool (Coombs et al., 1955; Gustafsson and Pinter, 1984a; Gustafsson and Pinter, 1984b; Powers and Binder, 2001), and that Ohm's law is followed in MNs (Glenn and Dement, 1981; Spruston and Johnston, 1992; Kernell, 2006). Finally, the findings $R \propto \tau^2, C \propto \frac{1}{\tau}$ and $R_m \propto \tau$ in Table 6 numerically validate the classic empirical relationship $\tau = RC = R_m C_m$ (Gustafsson and Pinter, 1984a; Zengel et al., 1985). From the typical ranges of values obtained from the literature for $\{\tau; C_m\}$ or $\{R; S_{MN}\}$, the latter relationship enforces $R_m \in [0.16; 0.62]\Omega \cdot m^2$, which is consistent with the ranges of R_m values speculated in (Albuquerque and Thesleff, 1968; Barrett and Crill, 1974; Burke et al., 1982; Gustafsson and Pinter, 1984a; Kernell and Zwaagstra, 1989) (Table 5).

Henneman's size principle of MU recruitment

Table 8 reports statistically significant power relationships $S_{mU} \propto S_{MN}^{c}$ of positive c-values between MN and mU indices of size. These results substantiate the concept that S_{MN} and S_{mU} are positively correlated in a MU pool and that large MNs innervate large mUs (Henneman, 1981; Heckman and Enoka, 2012), a statement that has never been demonstrated from the concurrent direct measurement of S_{MN} and S_{mU}. Besides, considering that $I_{th} \propto S_{MN}^{2}$ (Table 6), and that the mU force recruitment threshold F^{th} is positively correlated to F^{tet} (Heckman and Enoka, 2012) and thus to S_{mU} (Table 2), larger MUs have both larger current and force recruitment thresholds I_{th} and F^{th} than relatively smaller MUs, which are thus recruited first, consistently with the Henneman's size principle of MU recruitment (Henneman, 1957; Wuerker et al., 1965; Henneman et al., 1965a; Henneman et al., 1965b; Henneman et al., 1974; Henneman, 1981; Henneman, 1985). The terminologies 'small MU', 'low-force MU' and 'low-threshold MU' are thus equivalent. Henneman's size principle thus entirely relies on the amplitude of the MN membrane resistance $R \propto S_{MN}^{-2}$, as inferred in (Binder et al., 1996; Powers and Binder, 2001; Heckman and Enoka, 2012). Finally, the relationships $S_{MN} \propto CV^{0.6} \propto \tau^{-1} \propto AHP^{-1}$ (Table 6) suggest that high-threshold MUs rely on relatively faster MN dynamics, which might partially explain why large MNs can attain relatively larger firing rates than low-thresholds MNs.

It has been repeatedly attempted to extend Henneman's size principle and the correlations between the MU properties in Table 1 to the concept of 'MU type' (Burke and Ten Bruggencate, 1971; Burke, 1981; Bakels and Kernell, 1993; Powers and Binder, 2001). While a significant association between 'MU type' and indices of MU size has been observed in some animal (Fleshman et al., 1981; Burke et al., 1982; Zengel et al., 1985) and a few human (Milner-Brown et al., 1973; Stephens and Usherwood, 1977; Garnett et al., 1979; Andreassen and Arendt-Nielsen, 1987) studies, it has however not been observed in other animal studies ((Bigland-Ritchie et al., 1998) for a review) and in the majority of human investigations (Sica and McComas, 1971; Goldberg and Derfler, 1977; Yemm, 1977; Young and Mayer, 1982; Thomas et al., 1990; Nordstrom and Miles, 1990; Elek et al., 1992; Macefield et al., 1996; Cutsem et al., 1997; Mateika et al., 1998; Fuglevand et al., 1999; Keen and Fuglevand, 2004). Moreover, the reliability of these results is weakened by the strong limitations of the typical MU type identification protocols. Sag experiments are irrelevant in humans (Buchthal and Schmalbruch, 1970; Thomas et al., 1991; Bakels and Kernell, 1993; Macefield et al., 1996; Bigland-Ritchie et al., 1998; Fuglevand et al., 1999), and lack consistency with other identification methods (Nordstrom and Miles, 1990). MU type identification by twitch contraction time measurements is limited by the strong sources of inaccuracy involved in the transcutaneous stimulation, intramuscular microstimulation, intraneural stimulation, and spike-triggered averaging techniques (Taylor et al., 2002; Keen and Fuglevand, 2004; McNulty and Macefield, 2005; Negro et al., 2014; Dideriksen and Negro, 2018). Finally, as muscle fibres show a continuous distribution of contractile properties among the MU pool, some MUs fail to be categorized in discrete MU types in some animal studies by histochemical approaches (Reinking et al., 1975; Totosy de Zepetnek, J E et al., 1992). Owing to these conflicting results and technical limitations, MU type may not be related to MN size and the basis for MU recruitment during voluntary contractions (McNulty and Macefield, 2005; Duchateau and Enoka, 2011).

Limitations

The mathematical relationships derived Table 6 and the conclusions drawn in the Discussion are constrained by some limitations.

A first limitation is due to the limited experimental data available in the literature, as also discussed by Heckman and Enoka (2012). Some pairs of MN properties were investigated in only one study, such as $\{C; R\}$ or $\{\tau; AHP\}$, preventing inter-study comparisons. There have been no studies in the past 30 years on direct measures of these properties. Moreover, measurements obtained from different species (cat, rat) and different muscles were merged into unique datasets, implicitly assuming similar distributions of MN properties within the MN pool of different muscles and species.

A second limitation is related to the methods chosen for processing the retrieved data. The measurements were reproduced from a digitization of scatter plots, which may have determined small inaccuracies. All datasets were besides normalized to the highest measured value retrieved in each study; this approach is only valid if the experimental studies identified the same largest MN relatively to the MN populations under investigation, which cannot be verified.

Conclusion

This study provides the first empirical and algebraical proof that the MN size S_{MN} precisely determines all other MN properties (CV, AHP, R, I_{th}, C and τ). The derived mathematical relationships between any of these MN properties and/or S_{MN} are provided in Table 6. They accurately describe the experimental data available in the literature and provide for the first time a method for building virtual MN profiles of inter-consistent MN-specific properties.

References

Adrian RH, Hodgkin AL (1975) Conduction velocity and gating current in the squid giant axon. Proc. Royal Soc. B P ROY SOC B-BIOL SCI 189:81-86.

Albuquerque EX, Thesleff S (1968) A comparative study of membrane properties of innervated and chronically denervated fast and slow skeletal muscles of the rat. Acta Physiol. Scand. 73:471-480.

Andreassen S, Arendt-Nielsen L (1987) Muscle fibre conduction velocity in motor units of the human anterior tibial muscle: A new size principle parameter. J. Physiol. 391:561-571.

Ankit, R. (2020) WebPlotDigitizer. 4.4 https://automeris.io/WebPlotDigitizer.

Appelberg B, Emonet-Dénand F (1967) Motor units of the first superficial lumbrical muscle of the cat. J. Neurophysiol. 30:154-160.

Bagust J (1974) Relationships between motor nerve conduction velocities and motor unit contraction characteristics in a slow twitch muscle of the cat. J. Physiol. 238:269-278.

Bakels R, Kernell D (1993) Matching between motoneurone and muscle unit properties in rat medial gastrocnemius. J. Physiol. 463:307-324.

Barrett JN, Crill WE (1974) Specific membrane properties of cat motoneurones. J. Physiol. 239:301-324.

Bigland-Ritchie B, Fuglevand AJ, Thomas CK (1998) Contractile properties of human motor units: Is man a cat? The Neuroscientist 4:240-249.

Binder, M. D., Heckman, C. J. & Powers, R. K. (1996) The physiological control of motoneuron activity. In Rowell LB, S. J. (ed), *Handbook of Physiology: Exercise, Regulation and Integration of Multiple Systems.* New York: Oxford Univ Press, pp. 3-53.

Bodine SC, Roy RR, Eldred E, Edgerton VR (1987) Maximal force as a function of anatomical features of motor units in the cat tibialis anterior. J. Neurophysiol. 57:1730-1745.

Brock LG, Coombs JS, Eccles JC (1952) The recording of potentials from motoneurones with an intracellular electrode. J.Physiol.(Lond.) 117:431-460.

Buchthal F, Schmalbruch H (1970) Contraction times and fibre types in intact human muscle. Acta Physiol. Scand. 79:435-452.

Burke RE, Ten Bruggencate G (1971) Electrotonic characteristics of alpha motoneurones of varying size. J. Physiol. 212:1-20.

Burke RE, Dum RP, Fleshman JW, Glenn LL, Lev-Tov A, O'Donovan MJ, Pinter MJ (1982) An HRP study of the relation between cell size and motor unit type in cat ankle extensor motoneurons. J. Comp. Neurol. 209:17-28.

Burke RE, Tsairis P (1973) Anatomy and innervation ratios in motor units of cat gastrocnemius. J. Physiol. 234:749-765.

Burke RE (1968) Firing patterns of gastrocnemius motor units in the decerebrate cat. J. Physiol. 196:631-654.

Burke, R. E. (1981) Motor units: Anatomy, physiology, and functional organization. In Brooks, V. B. (ed), *Handbook of Physiology, the Nervous System, Motor Control.* American Physiological Society, pp. 345-422.

Chamberlain S, Lewis DM (1989) Contractile characteristics and innervation ratio of rat soleus motor units. J. Physiol. 412:1-21.

Coombs JS, Eccles JC, Fatt P (1955) The electrical properties of the motoneurone membrane. J.Physiol.(Lond.) 130:291-325.

Cullheim S (1978) Relations between cell body size, axon diameter and axon conduction velocity of cat sciatic α-motoneurons stained with horseradish peroxidase. Neurosci. Lett. 8:17-20.

Cutsem MV, Feiereisen P, Duchateau J, Hainaut K (1997) Mechanical properties and behaviour of motor units in the tibialis anterior during voluntary contractions. Can. J. Appl. Physiol. 22:585-597.

Dengler R, Stein RB, Thomas CK (1988) Axonal conduction velocity and force of single human motor units. Muscle & Nerve: Official Journal of the American Association of Electrodiagnostic Medicine 11:136-145.

Dideriksen JL, Negro F (2018) Spike-triggered averaging provides inaccurate estimates of motor unit twitch properties under optimal conditions. J Electromyogr Kinesiol 43:104-110.

Duchateau J, Enoka RM (2011) Human motor unit recordings: Origins and insight into the integrated motor system. Brain Res. 1409:42-61.

Dum RP, Kennedy TT (1980) Physiological and histochemical characteristics of motor units in cat tibialis anterior and extensor digitorum longus muscles. J. Neurophysiol. 43:1615-1630.

Eccles JC, Libet B, Young RR (1958) The behaviour of chromatolysed motoneurones studied by intracellular recording. J.Physiol.(Lond.) 143:11-40.

Eccles JC, Eccles RM, Lundberg A (1957) Durations of after-hyperpolarization of motoneurones supplying fast and slow muscles. Nature 179:866-868.

Elek JM, Kossev A, Dengler R, Schubert M, Wohlfahrt K, Wolf W (1992) Parameters of human motor unit twitches obtained by intramuscular microstimulation. Neuromuscul. Disord. 2:261-267.

Emonet-Dénand F, Hunt CC, Petit J, Pollin B (1988) Proportion of fatigue-resistant motor units in hindlimb muscles of cat and their relation to axonal conduction velocity. J. Physiol. 400:135-158.

Enoka RM (1995) Morphological features and activation patterns of motor units. J Clin Neurophysiol 12:538-559.

Fleshman JW, Munson JB, Sypert GW, Friedman WA (1981) Rheobase, input resistance, and motor-unit type in medial gastrocnemius motoneurons in the cat. J Neurophysiol 46:1326-1338.

Foehring RC, Sypert GW, Munson JB (1987) Motor-unit properties following cross-reinnervation of cat lateral gastrocnemius and soleus muscles with medial gastrocnemius nerve. II. influence of muscle on motoneurons. J Neurophysiol 57:1227-1245.

Foehring RC, Sypert GW, Munson JB (1986) Properties of self-reinnervated motor units of medial gastrocnemius of cat. II. axotomized motoneurons and time course of recovery. J Neurophysiol 55:947-965.

Freund HJ, Budingen HJ, Dietz V (1975) Activity of single motor units from human forearm muscles during voluntary isometric contractions. J.Neurophysiol. 38:933-946.

Fuglevand AJ, Macefield VG, Bigland-Ritchie B (1999) Force-frequency and fatigue properties of motor units in muscles that control digits of the human hand. J Neurophysiol 81:1718-1729.

Gardiner PF (1993) Physiological properties of motoneurons innervating different muscle unit types in rat gastrocnemius. J Neurophysiol 69:1160-1170.

Garnett RAF, O'Donovan MJ, Stephens JA, Taylor A (1979) Motor unit organization of human medial gastrocnemius. J. Physiol. 287:33-43.

Gentet L, Stuart GJ, Clements JD (2000) Direct measurement of specific membrane capacitance in neurons. Biophys. J. 79:314-320.

Glenn LL, Dement WC (1981) Membrane resistance and rheobase of hindlimb motoneurons during wakefulness and sleep. J Neurophysiol 46:1076-1088.

Goldberg LJ, Derfler B (1977) Relationship among recruitment order, spike amplitude, and twitch tension of single motor units in human masseter muscle. J Neurophysiol 40:879-890.

Gustafsson B, Pinter MJ (1985) On factors determining orderly recruitment of motor units: A role for intrinsic membrane properties. Trends Neurosci. 431-433.

Gustafsson B, Pinter MJ (1984a) Relations among passive electrical properties of lumbar alpha-motoneurones of the cat. J. Physiol. 356:401-431.

Gustafsson B, Pinter MJ (1984b) An investigation of threshold properties among cat spinal alpha-motoneurones. J. Physiol. 357:453-483.

Gustafsson B (1979) Changes in motoneurone electrical properties following axotomy. J. Physiol. 293:197-215.

Heckman CJ, Enoka RM (2012) Motor unit. Compr. Physiol. 2:2629-2682.

Henneman E (1985) The size-principle: A deterministic output emerges from a set of probabilistic connections. J. Exp. Biol. 115:105-112.

Henneman E (1981) Recruitment of motoneurons : The size principle. Motor Unit Types, Recruitment and Plasticity in Health and Disease 26-60.

Henneman E, Clamann HP, Gillies JD, Skinner RD (1974) Rank order of motoneurons within a pool: Law of combination. J Neurophysiol 37:1338-1349.

Henneman E, Somjen G, Carpenter DO (1965a) Functional significance of cell size in spinal motoneurons. J Neurophysiol 28:560-580.

Henneman E, Somjen G, Carpenter DO (1965b) Excitability and inhibitibility of motoneurons of different sizes. J Neurophysiol 28:599-620.

Henneman E (1957) Relation between size of neurons and their susceptibility to discharge. Science 126:1345-1347.

Jami L, Petit J (1975) Correlation between axonal conduction velocity and tetanic tension of motor units in four muscles of the cat hind limb. Brain Res. 96:114-118.

Kanda K, Hashizume K (1992) Factors causing difference in force output among motor units in the rat medial gastrocnemius muscle. J. Physiol. 448:677-695.

Keen DA, Fuglevand AJ (2004) Distribution of motor unit force in human extensor digitorum assessed by spike-triggered averaging and intraneural microstimulation. J Neurophysiol 91:2515-2523.

Kernell D (2006) *The Motoneurone and its Muscle Fibres.* Oxford University Press UK, .

Kernell D, Zwaagstra B (1989) Dendrites of cat's spinal motoneurones: Relationship between stem diameter and predicted input conductance. J. Physiol. 413:255-269.

Kernell D, Monster AW (1981) Threshold current for repetitive impulse firing in motoneurones innervating muscle fibres of different fatigue sensitivity in the cat. Brain Res. 229:193-196.

Kernell D, Zwaagstra B (1981) Input conductance, axonal conduction velocity and cell size among hindlimb motoneurones of the cat. Brain Res. 204:311-326.

Kernell D (1966) Input resistance, electrical excitability, and size of ventral horn cells in cat spinal cord. Science 152:1637-1640.

Lucas SM, Ruff RL, Binder MD (1987) Specific tension measurements in single soleus and medial gastrocnemius muscle fibers of the cat. Exp.Neurol. 95:142-154.

Lux HD, Pollen DA (1966) Electrical constants of neurons in the motor cortex of the cat. J.Neurophysiol. 29:207-220.

Macefield VG, Fuglevand AJ, Bigland-Ritchie B (1996) Contractile properties of single motor units in human toe extensors assessed by intraneural motor axon stimulation. J Neurophysiol 75:2509-2519.

Major G, Larkman AU, Jonas P, Sakmann B, Jack JJ (1994) Detailed passive cable models of whole-cell recorded CA3 pyramidal neurons in rat hippocampal slices. J.Neurosci. 14:4613-4638.

Mateika JH, Essif EG, Dellorusso C, Fregosi RF (1998) Contractile properties of human nasal dilator motor units. J Neurophysiol 79:371-378.

McNulty PA, Macefield VG (2005) Intraneural microstimulation of motor axons in the study of human single motor units. Muscle & Nerve: Official Journal of the American Association of Electrodiagnostic Medicine 32:119-139.

McPhedran AM, Wuerker RB, Henneman E (1965) Properties of motor units in a homogeneous red muscle (soleus) of the cat. J Neurophysiol 28:71-84.

Milner-Brown HS, Stein RB, Yemm R (1973) The orderly recruitment of human motor units during voluntary isometric contractions. J. Physiol. 230:359-370.

Negro F, Yavuz U, Farina D (2016) The human motor neuron pools receive a dominant slow-varying common synaptic input. J. Physiol. 594:5491-5505.

Negro F, Yavuz U, Farina D (2014) Limitations of the spike-triggered averaging for estimating motor unit twitch force: A theoretical analysis. PloS one 9:e92390.

Nordstrom MA, Miles TS (1990) Fatigue of single motor units in human masseter. J. Appl. Physiol. 68:26-34.

Olson CB, Swett Jr CP (1966) A functional and histochemical characterization of motor units in a heterogeneous muscle (flexor digitorum longus) of the cat. J. Comp. Neurol. 128:475-497.

Powers RK, Binder MD (2001) Input-output functions of mammalian motoneurons. Rev. Physiol. Biochem. Pharmacol. 143:137-263.

Proske U, Waite PME (1974) Properties of types of motor units in the medial gastrocnemius muscle of the cat. Brain Res. 67:89-101.

Rafuse VF, Pattullo MC, Gordon T (1997) Innervation ratio and motor unit force in large muscles: A study of chronically stimulated cat medial gastrocnemius. J. Physiol. 499:809-823.

Rall W (1960) Membrane potential transients and membrane time constant of motoneurons. Exp.Neurol. 2:503-532.

Rall W (1959) Branching dendritic trees and motoneuron membrane resistivity. Exp.Neurol. 1:491-527.

Rall W (1957) Membrane time constant of motoneurons. Science 126:454.

Reinking RM, Stephens JA, Stuart DG (1975) The motor units of cat medial gastrocnemius: Problem of their categorisation on the basis of mechanical properties. Exp. Brain Res. 23:301-313.

Sica REP, McComas AJ (1971) Fast and slow twitch units in a human muscle. J. Neurol. Neurosurg. Psychiatry 34:113-120.

Solsona C, Innocenti B, Fernández JM (1998) Regulation of exocytotic fusion by cell inflation. Biophys.J. 74:1061-1073.

Spruston N, Johnston D (1992) Perforated patch-clamp analysis of the passive membrane properties of three classes of hippocampal neurons. J Neurophysiol 67:508-529.

Stephens JA, Stuart DG (1975) The motor units of cat medial gastrocnemius: Speed-size relations and their significance for the recruitment order of motor units. Brain. Res. 91:177-195.

Stephens JA, Usherwood TP (1977) The mechanical properties of human motor units with special reference to their fatiguability and recruitment threshold. Brain Res. 125:91-97.

Sukhorukov VL, Arnold WM, Zimmermann U (1993) Hypotonically induced changes in the plasma membrane of cultured mammalian cells. J.Membr.Biol. 132:27-40.

Taylor AM, Steege JW, Enoka RM (2002) Motor-unit synchronization alters spike-triggered average force in simulated contractions. J Neurophysiol 88:265-276.

Teeter C, Iyer R, Menon V, Gouwens N, Feng D, Berg J, Szafer A, Cain N, Zeng H, Hawrylycz M, Koch C, Mihalas S (2018) Generalized leaky integrate-and-fire models classify multiple neuron types. Nat Commun 9:1-15.

Thomas CK, Bigland-Richie B, Johansson RS (1991) Force-frequency relationships of human thenar motor units. J. Neurophysiol. 65:1509-1516.

Thomas CK, Johansson RS, Westling G, Bigland-Ritchie B (1990) Twitch properties of human thenar motor units measured in response to intraneural motor-axon stimulation. J Neurophysiol 64:1339-1346.

Thurbon D, Hans-R. Lüscher, Hofstetter T, Redman SJ (1998) Passive electrical properties of ventral horn neurons in rat spinal cord slices. J.Neurophysiol. 79:2485-2502.

Totosy de Zepetnek, J E, Zung HV, Erdebil S, Gordon T (1992) Innervation ratio is an important determinant of force in normal and reinnervated rat tibialis anterior muscles. J Neurophysiol 67:1385-1403.

Ulfhake B, Kellerth JO (1984) Electrophysiological and morphological measurements in cat gastrocnemius and soleus α-motoneurones. Brain Res. 307:167-179.

Ulfhake B, Kellerth JO (1981) A quantitative light microscopic study of the dendrites of cat spinal α-motoneurons after intracellular staining with horseradish peroxidase. J. Comp. Neurol. 202:571-583.

Wuerker RB, McPhedran AM, Henneman E (1965) Properties of motor units in a heterogeneous pale muscle (m. gastrocnemius) of the cat. J.Neurophysiol. 28:85-99.

Yemm R (1977) The orderly recruitment of motor units of the masseter and temporal muscles during voluntary isometric contraction in man. J. Physiol. 265:163-174.

Young JL, Mayer RF (1982) Physiological alterations of motor units in hemiplegia. J. Neurol. Sci. 54:401-412.

Zengel JE, Reid SA, Sypert GW, Munson JB (1985) Membrane electrical properties and prediction of motor-unit type of medial gastrocnemius motoneurons in the cat. J Neurophysiol 53:1323-1344.

Zwaagstra B, Kernell D (1980) The duration of after-hyperpolarization in hindlimb alpha motoneurones of different sizes in the cat. Neurosci. Lett. 19:303-307.